JASS Journal of Astronomy and Space Sciences

A Study of Dark Photon at the Electron-Positron Collider Experiments Using KISTI-5 Supercomputer

Kihong Park[1,2], Kihyeon Cho[1,2†]

[1]University of Science and Technology, Daejeon 34113, Korea
[2]Korea Institute of Science and Technology Information, Daejeon 34141, Korea

The universe is well known to be consists of dark energy, dark matter and the standard model (SM) particles. The dark matter dominates the density of matter in the universe. The dark matter is thought to be linked with dark photon which are hypothetical hidden sector particles similar to photons in electromagnetism but potentially proposed as force carriers. Due to the extremely small cross-section of dark matter, a large amount of data is needed to be processed. Therefore, we need to optimize the central processing unit (CPU) time. In this work, using MadGraph5 as a simulation tool kit, we examined the CPU time, and cross-section of dark matter at the electron-positron collider considering three parameters including the center of mass energy, dark photon mass, and coupling constant. The signal process pertained to a dark photon, which couples only to heavy leptons. We only dealt with the case of dark photon decaying into two muons. We used the simplified model which covers dark matter particles and dark photon particles as well as the SM particles. To compare the CPU time of simulation, one or more cores of the KISTI-5 supercomputer of Nurion Knights Landing and Skylake and a local Linux machine were used. Our results can help optimize high-energy physics software through high-performance computing and enable the users to incorporate parallel processing.

Keywords: dark matter, dark photon, high-energy physics, electron-positron collider, computational science, high-performance computing

1. INTRODUCTION

The universe is well known to be consists of 70% dark energy, 26% dark matter and 4% the standard model (SM) particles (Cho 2016a, b). The dark matter dominates the density of matter in the universe, but the particles have not been detected directly or indirectly until now. Considering the rich interaction structure of the SM particles that well describe the composition of the universe, it is natural to think of similar interaction behaviors of dark-sector particles. Dark photons can be part of this interaction between dark matter particles and provide the presence of a non-gravitational force window by kinematically mixed with the SM photons (Choi 2018). Computational science is being widely applied in the area of astroparticle physics, especially in the search for dark matter (Cho 2016a, b; Cho

2017). Because the cross-section of dark matter is extremely small compared to that calculated by the SM, extensive simulations are required (Cho 2017) in such analyses. In this regard, it is necessary to optimize the central processing unit (CPU) time to efficiently carry out simulations (Cho 2017; Yeo & Cho 2019; Yeo & Cho 2020). The SM has been well-established with the discovery of the Higgs boson particle (Aad et al. 2012; Chatrchyan et al. 2012). However, because the SM does not explain the characteristics of dark matter, little is known about it and it is being actively investigated through various methods (Cho 2016a).

In this work, we studied dark matter at the electron-positron collider using MadGraph5 as a simulation tool (Alwall et al. 2014; Yeo & Cho 2018). Specifically, we examined the CPU time and cross-section values considering three parameters such as the center of mass (CM) energy,

dark photon mass, and coupling constant. The signal process corresponded to the dark photon, which couples only with heavy leptons (Shuve & Yavin 2014; Yeo & Cho 2018). We only dealt with the case of dark photon decaying into two muons using simplified model which covers the SM particles, dark matter particles, and dark photon particles (Alves et al. 2012). To compare the CPU time for the corresponding calculation, the KISTI-5 supercomputer of Nurion Knights Landing (KNL) and Skylake (SKL) and a local Linux machine were employed. The Nurion KNL and the SKL are equipped with the Intel Xeon Phi 7250 and Xeon 6148 processors with 68 and 40 cores per node, respectively. One or more cores of the machines were used to compare the CPU time.

2. METHODS

This section presents the specifications of the Nurion KNL, the Nurion SKL, and the local Linux machine (Yeo & Cho 2020). The machines were used to compare the CPU time under the same sample jobs. The Nurion KNL and the SKL consist of 8305 and 132 nodes, with each node having 68 and 40 cores, respectively. The local Linux machine has 32 cores. The theoretical peak performance for the Nurion machine is 25.7 PFLOPS (with the KNL and the SKL corresponding to 25.3 and 0.4 PFLOPS, respectively) (Yeo & Cho 2020). Table 1 summarize the specifications of the employed machines. Fig. 1 shows the process flow of the complete simulation (Cho 2016a, b). We generated the electron-positron collider event at a CM energy ranging from 10 GeV to 500 GeV. This energy range was selected considering the requirements of Belle II (10.58 GeV) , Future Circular Collider (FCC)-ee (91 GeV), FCC-ee/Circular Electron-Positron Collider (CEPC) (160 GeV), CEPC (240 GeV), and International Linear Collider (ILC) (500 GeV) which pertain to representative electron-positron collider experiments. Feynman diagrams were generated using MadGraph5 (Alwall et al. 2014) from the simplified model (Alves et al. 2012), and the event simulation was performed
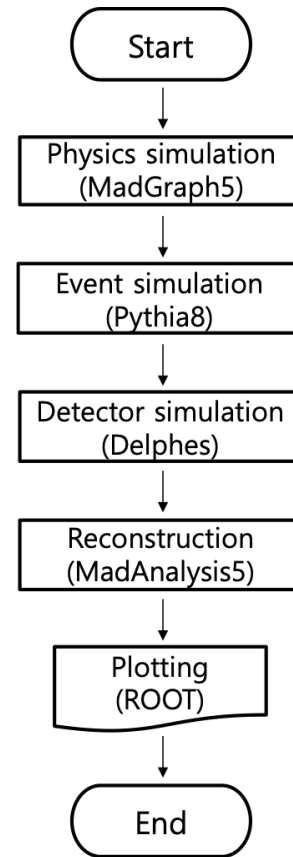

Fig. 1. Process flow of the simulation.

on the Pythia8 framework (Sjöstrand et al. 2015). Next, the detector simulation was performed using Delphes (de Favereau et al. 2014). Finally, physics reconstruction was performed using MadAnalysis5 (Conte et al. 2013). The result file was generated in the ROOT format for plotting (Antcheva 2009).

3. DARK PHOTON AT THE ELECTRON-POSITRON COLLIIDER

If the dark photons in the dark sector interact with the

Table 1. Specification of the KISTI-5 supercomputer and the local Linux machine

Specification	KISTI-5 KNL	KISTI-5 SKL	Local Linux machine
OS	CentOS7.4	CentOS7.4	Scientific Linux 6.5
Processor	Intel Xeon Phi 7250 1.4 GHz	Intel Xeon Skylake (Gold 6148) 2.4 GHz	Intel Xeon CPU X5560 2.8 GHz
Architecture	Many-core	Multicore	Multicore
Number of cores/CPU	68	20	4
Number of CPUs/node	1	2	8
Number of cores/node	68	40	32
Number of total nodes	8,305	132	1
Number of total cores	564,740	5,280	32

CPU, central processing unit.

particles of the SM, the dark photon can be coupled with charged lepton, that is muon, which corresponds to dark sector type 4 (Shuve & Yavin 2014; Yeo & Cho 2018). The signal process is $e^+ e^- \to \mu^+ \mu^- A'$ with a dark photon $A' \to \mu^+ \mu^-$. This theory can explain the anomalous muon magnetic moment (Shuve & Yavin 2014). If the dark photon mass is less than the masses of the two muons, the dark photon decays into two neutrinos or two dark matter particles. These objects are transformed into missing transverse energy (MET) without a trace on the detector. The simplified model is adopted as the theoretical model in this study (Alves et al. 2012). The model is intermediate to the ultraviolet (UV) model and effective field theory. The UV model includes supersymmetry (SUSY) particles and extra dimensions, whereas the effective field theory includes SM and dark matter particles. The simplified model includes both the SM particles and dark matter particles as well as mediator particles. The simplified model is primarily used when generating signal events. Because several parameters are associated with the signal process, we examined the dependence of the parameters by plotting cross-section graphs.

3.1 The Standard Model as a Background

The most dominant backgrounds correspond to the SM. The mode is $e^+ e^- \to \mu^+ \mu^- \mu^+ \mu^-$. Table 2 presents the settings for the SM event generation. The local Linux machine was adopted. The events were generated using MadGraph5 v2.6.4 with the default parameter card, Pythia8 (Sjöstrand et al. 2015), default Delphes (de Favereau et al. 2014), and MadAnalysis5 (Conte et al. 2013). We generated four muon final states for the SM. The number of events per run was

Table 2. Settings for the standard model (SM) event generation

Specification	Content
Machine	Local Linux machine
Simulation tool kit	MadGraph5 v2.6.4
Software	Pythia8, Delphes (CMS), MadAnalysis5
Command	generate e+ e– > mu+ mu– mu+ mu–
Number of events	10,000
CM energy	50, 60, ..., 490, 500 GeV

CMS, compact muon solenoid; CM, center of mass.

10,000. The CM energy increased from 50 GeV to 500 GeV by 10 GeV. Events with a CM energy of less than 40 GeV were not generated because of the zero cross-section.

The mediator particles in all the Feynman diagrams were photons or Z bosons. Fig. 2 shows the cross-section of the SM event depending on CM energies. A total of 48 modes are involved in the process.

Fig. 3 shows the dominant modes of the SM. Mode 1 contributed to the first peak that occurred at approximately 90 GeV, attributable to the Z boson interaction. The second peak, which occurred near 210 GeV, corresponded to the maximum cross-section. This peak could be attributed to the presence of two Z bosons as mediator particles.

3.2 Dark Photon Signal Process

The signal process was $e^+ e^- \to \mu^+ \mu^- A'$ with $A' \to \mu^+ \mu^-$. When the CM energy was less than 30 GeV, the process of the photon or Z boson interaction was applied, as these interactions are dominant in this CM energy range. Because three parameters are involved in the generation of signal events, we examined the dependence of the cross-section on each parameter sequentially. As shown in Fig. 4, four coupling constants exist in the signal process. The coupling
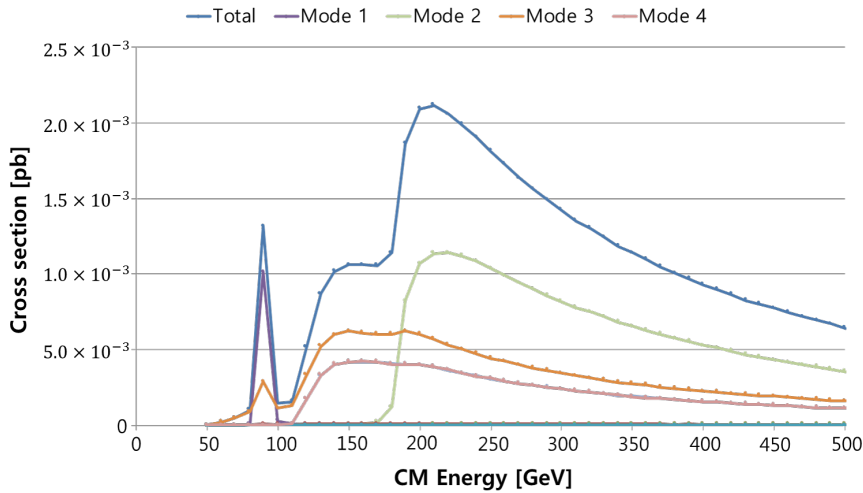

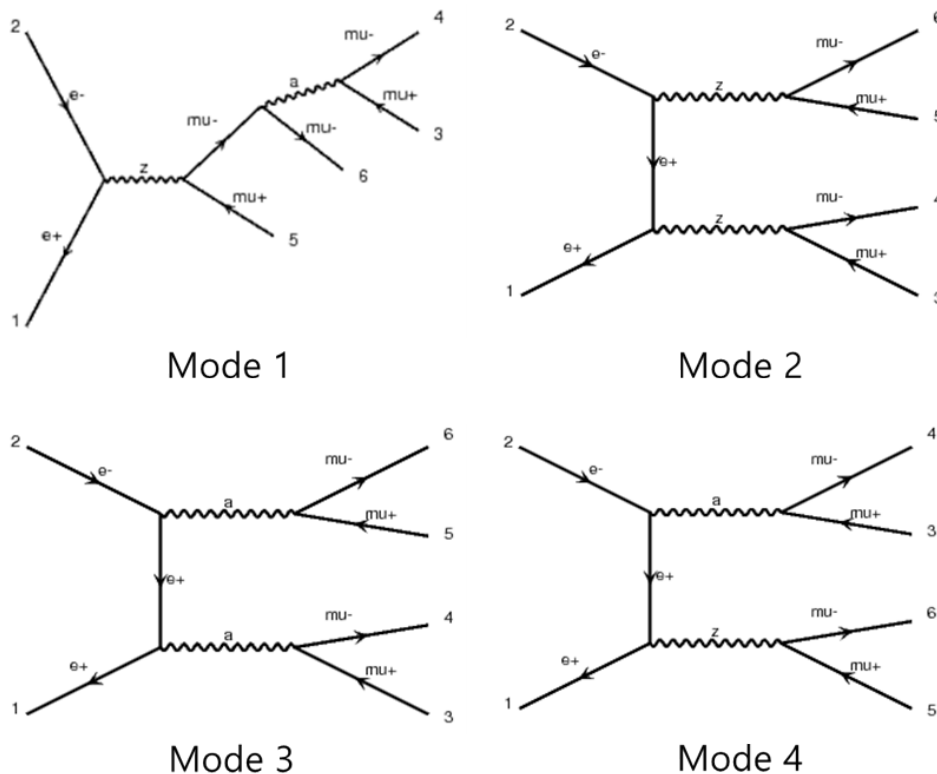**Fig. 2.** Standard model (SM) cross-section for different center of mass (CM) energies.

Fig. 3. The Feynman diagrams of dominant modes of the standard model.
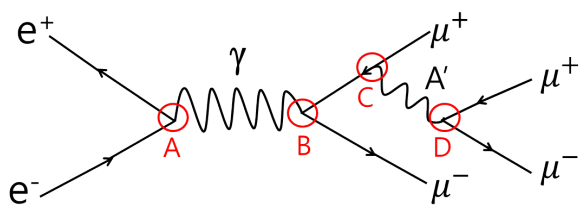

Fig. 4. Feynman diagram illustrating the coupling constants.

Table 4. Settings for the signal event generation

Specification	Content
Machine	Local Linux machine
Simulation tool kit	MadGraph5 v2.6.4
Softwares	Pythia8, Delphes (CMS), MadAnalysis5
Importing model	DMsimp_s_spin1
Command for process (a)	generate e+ e− > a, (a > mu+ mu− y1, y1 > mu+ mu−)
Command for process (b)	generate e+ e− > mu+ mu− y1, y1 > mu+ mu−
Number of events	10,000

CMS, compact muon solenoid.

constants are specified in Table 3. A and B correspond to electromagnetic coupling mediated by photon while C and D correspond to the coupling of muon and dark photon, respectively.

The signal events were generated using the settings listed in Table 4. Fig. 5 shows the Feynman diagrams of the signal event. Two processes were considered: (a) $e^+ e^- \rightarrow \gamma \rightarrow \mu^+ \mu^- A'$ with $A' \rightarrow \mu^+ \mu^-$ and (b) $e^+ e^- \rightarrow \mu^+ \mu^- A'$ with $A' \rightarrow \mu^+ \mu^-$.

Only process (a) had appeared when the CM energy was less than 30 GeV.

3.2.1 Cross-Section Dependence on the CM Energy

The CM energy increased from 10 GeV to 500 GeV by 10 GeV steps. The dark photon mass was fixed at 0.3 GeV and
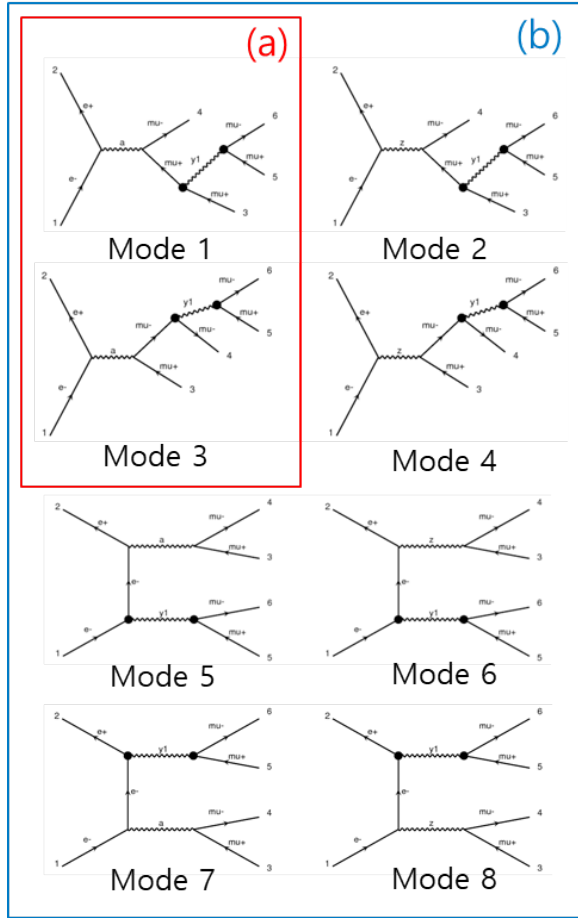
Table 3. Identification of the coupling constants

	Theory	MadGraph5	Default value	Description
A	α_{EW}^{-1}	aEWM1	1.325070×10^2	Inverse of the electromagnetic coupling
B	α_{EW}^{-1}	aEWM1	1.325070×10^2	Inverse of the electromagnetic coupling
C	$g_{l_{22}}^v$	gvl22	1	Muon-Y1 vector (dark photon) coupling
D	$g_{l_{22}}^v$	gvl22	1	Muon-Y1 vector (dark photon) coupling

Fig. 5. The possible Feynman diagrams of the signal mode.

(a) and (b), respectively. The cross-section of mode 3 and mode 4 is zero. The cross-section of mode 5 and mode 7 are overlayed. Likewise, the cross-section of mode 6 and mode 8 are overlayed.

3.2.2 Cross-Section Dependence on the Dark Photon Mass

Fig. 7 shows the cross-section variation with the dark photon mass (my1). The coupling constant was set as 0.1. The dark photon mass was varied from 1 KeV to 100 GeV and the CM energy was fixed at 10.58 GeV, 91 GeV, 160 GeV, 240 GeV, and 500 GeV. For the CM energy of 10.58 GeV and 91 GeV, the cross-section increased as the dark photon mass decreased. For the CM energy of 160 GeV, 240 GeV, and 500 GeV, the peak occurred when the dark photon mass was 50 GeV, 100 GeV, and 250 GeV, respectively. The red circle in the Fig. 7 indicates peaks due to the Z boson interaction.

3.2.3 Cross-Section Dependence on the Coupling Constant

The coupling constant of the muon and dark photon (gvl22) was varied and the coupling constant of the SM (aEWM1) was used as the default value. As shown in Fig. 8, the coupling constant varied from 0.01 to 1. The cross-section increased as the coupling constant increased.

We also checked the dependence of both CM energy and dark photon mass and the dependence of both dark photon mass and coupling constant.

the coupling constant was 1. At energies less than 30 GeV, process (a) was implemented. As shown in Fig. 6, the cross-section was maximized at the Z boson mass of 90 GeV. The most dominant modes were modes 1 and 8 in processes

4. RESULTS

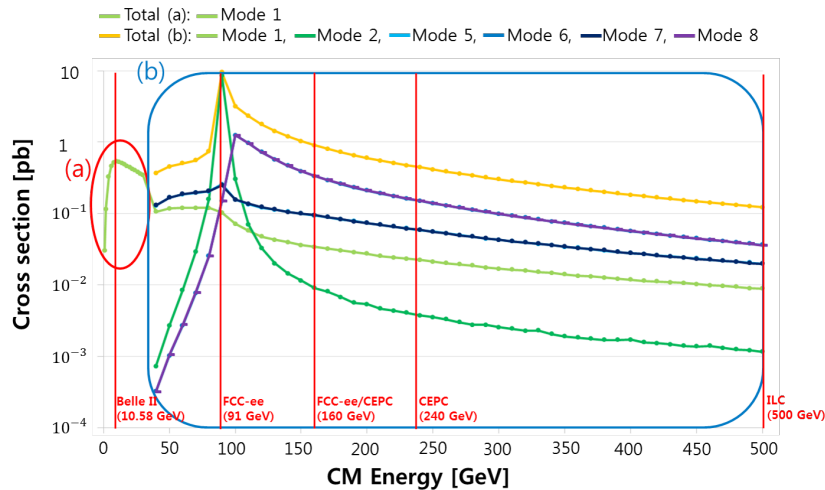We optimized the simulation tool kit by comparing the

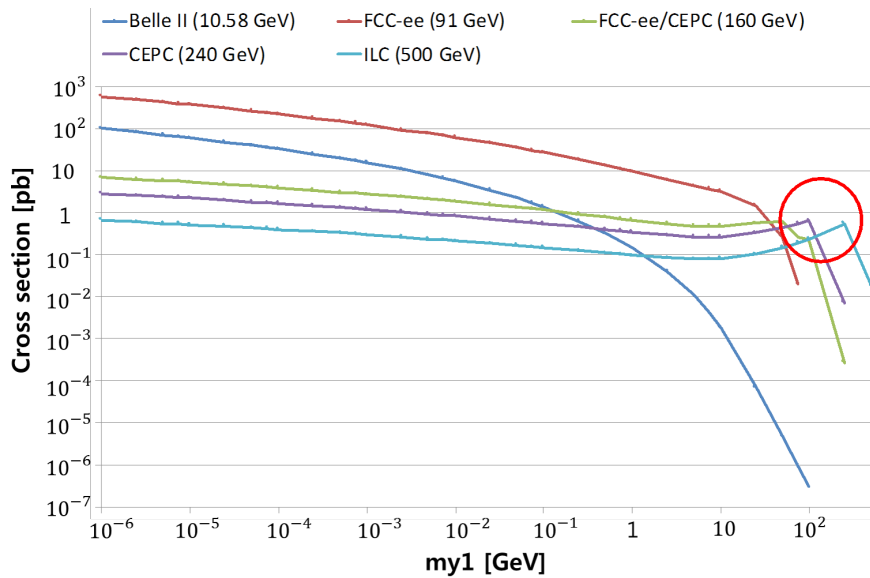**Fig. 6.** Cross-section dependence on the center of mass (CM) energy. CM, center of mass.

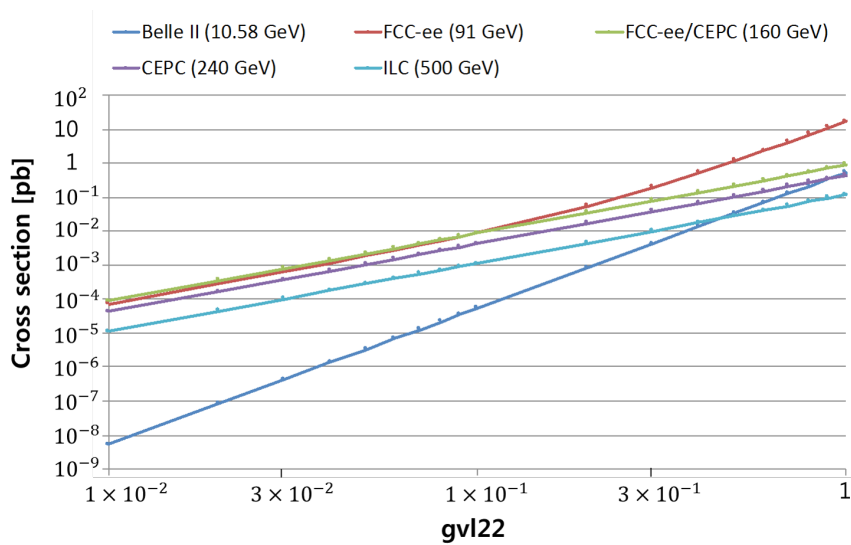**Fig. 7.** Dependence of cross-section on the dark photon mass.

Fig. 8. Dependence of the cross-section on the coupling constant.

time consumed by the CPU for various physics modes. Three cases were considered. The first case is that only the physics simulation was considered. The second case is the full simulation using Pythia8, Delphes, and MadAnalysis5 as well as the physics simulation. The third case is the examination of the efficiency of parallel processing among the machines. Table 5 describes the configuration of three cases: physics simulation only, full simulation, and physics simulation with parallel processing.

In the first case, events were generated from Feynman diagram using MadGraph5. The number of events was 10,000. The CM energy was 10.58 GeV (7 and 4 GeV for the

electron and positron, respectively). 15 jobs were submitted to be performed through parallel processing across all three machines. The coupling constant, gvl22, was 0.1. Fig. 9 shows the results of the CPU time and wall clock time when using the KNL, the SKL, and the local Linux machine. One core was used to determine the CPU time and wall clock time. Moreover, one node (68, 40, and 32 cores for the KNL, the SKL, and the local Linux machine, respectively) was used to determine the wall clock time. The CPU time was found to be greater than the wall clock time for all three machines. Comparing the performance of a single core with physics simulation, it was noted that the CPU of the

Table 5. The configuration for three cases

Item		Physics simulation only	Full simulation	Physics simulation with parallel processing
Simulation tool kit		MadGraph5 v2.6.4	MadGraph5 v2.6.4	MadGraph5 v2.6.4
Physics simulation		On	On	On
Pythia8, Delphes (CMS), MadAnalysis5		Off	On	Off
Importing model		DMsimp_s_spin1	DMsimp_s_spin1	DMsimp_s_spin1
Process		$e^+ e^- \to \gamma \to \mu^+ \mu^- A'$ with $A' \to \mu^+ \mu^-$	$e^+ e^- \to \gamma \to \mu^+ \mu^- A'$ with $A' \to \mu^+ \mu^-$	$e^+ e^- \to \gamma \to \mu^+ \mu^- A'$ with $A' \to \mu^+ \mu^-$
Number of events		10,000	10,000	10,000
CM energy		10.58 GeV	10.58 GeV	10.58 GeV
Dark photon mass		0.01 GeV	0.01 GeV	0.01 GeV
Coupling constant		0.1	0.1	0.1
No. of jobs	KNL	15	15	1, 3, 6, …, 60, 63, 66
	SKL	15	15	1, 3, 6, …, 27, 30, 33
	Local machine	15	15	1, 3, 6, 9, 12, 15

CMS, compact muon solenoid; CM, center of mass.
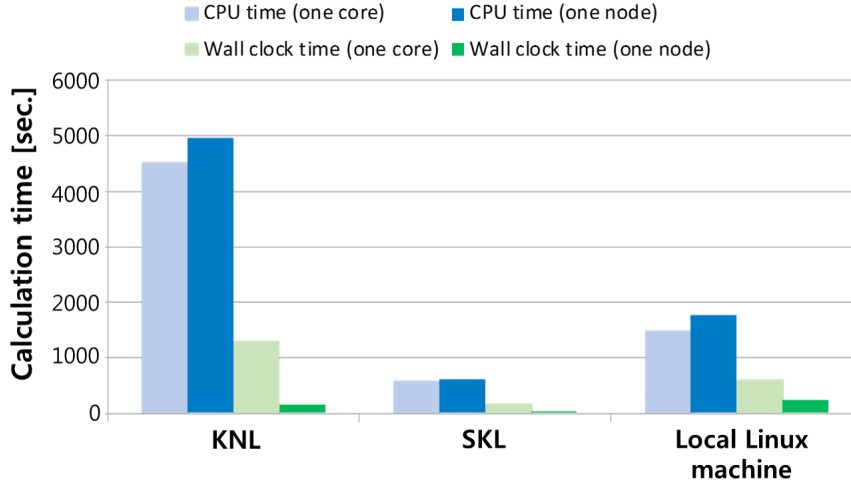
Fig. 9. CPU time and wall clock time with one core or more cores for different machines in the case of only the physics simulation. CPU, central processing unit.

SKL was faster than that of the KNL and the local Linux machine by a factor of 8.0 and 2.6, respectively. In terms of the wall clock time, the SKL was faster than the KNL and the local Linux machine by a factor of 7.3 and 3.4, respectively. Compared with the one node case, the wall clock time of one node (multiple cores) of the KNL, the SKL, and the local Linux machine was reduced by a factor of 8.6, 4.5, and 2.5, respectively. This result indicates that the efficiency of parallel processing for 15 jobs of the KNL and the SKL was higher than that of the local Linux machine.

In the second case, Pythia8, Delphes, and MadAnalysis5 software were employed. The number of events was 10,000. The dark photon mass was 0.01 GeV and coupling constant (gvl22) was 0.1. One job with one core was submitted. Fig. 10 shows the CPU time and wall clock time on the KNL, the SKL, and the local Linux machine. In terms of the wall clock time, the local Linux machine was found to be faster than the KNL

and the SKL by a factor of 5.3 and 1.0, respectively.

Moreover, in the third case, the efficiencies of parallel processing among machines were examined. The Pythia8, Delphes, and MadAnalysis5 software were not employed in this case. The number of events was 10,000. The used dark photon mass is 0.01 GeV and the coupling constant (gvl22) was 0.1. Fig. 11 shows the CPU time and wall clock time depending on the number of jobs among the machines denoted by (a) and (b) respectively. The higher efficiency of parallel processing corresponded to a smaller slope. In the ideal case, the slope is expected to be zero for the highest efficiency of parallel processing. Fig. 11 (a) indicates that the efficiency of parallel processing with the KNL is lower than that of the SKL and the local Linux machine in terms of CPU time. Fig. 11 (b) indicates that the parallel processing efficiency of the local Linux machine was lower than that of the KNL and the SKL in terms of the wall clock time.
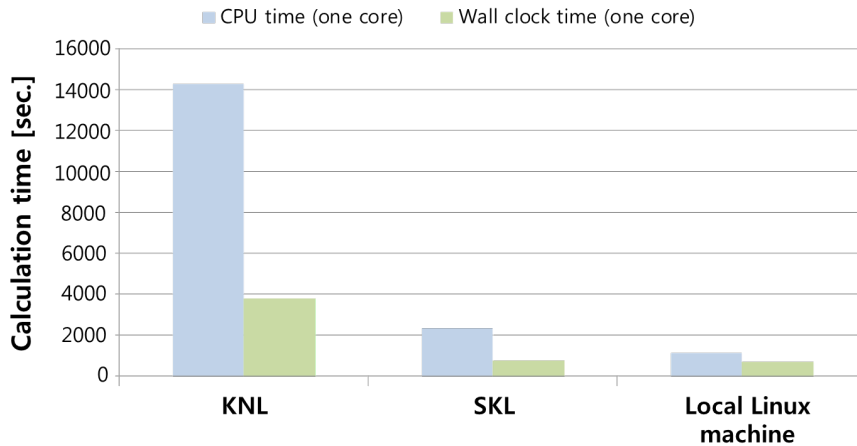
Fig. 10. CPU time and wall clock time with one core for different machines with the full simulation. CPU, central processing unit.
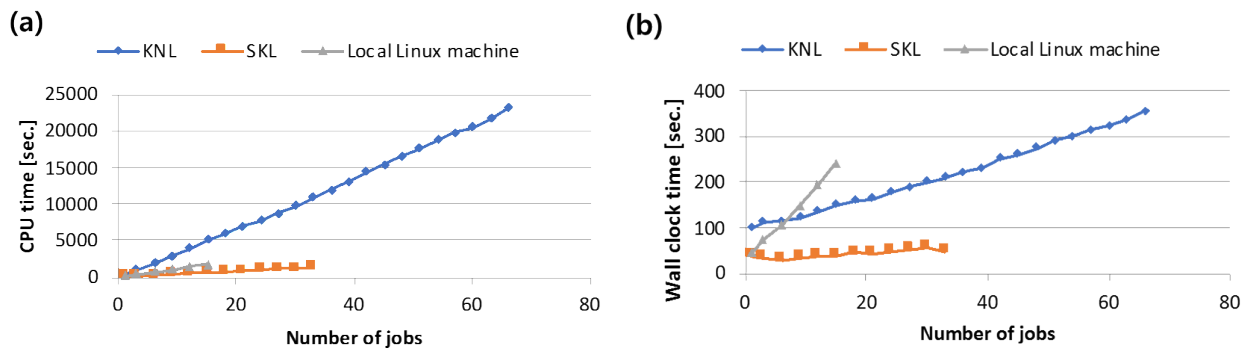
(a)

(b)

Fig. 11. CPU time and wall clock time depending on the number of jobs among machines denoted by (a) and (b) respectively. CPU, central processing unit.

The efficiency of parallel processing of the SKL was higher than that of the KNL. This result shows that although the performance of one core of the KNL was lower than that of the local Linux machine, the efficiency of parallel processing with a large number of the KNL cores was higher than that for the local Linux machine. Therefore, optimization and parallelization must be considered.

5. CONCLUSION

We have compared the CPU time using the KISTI-5 supercomputer (the Nurion KNL and the SKL) and the local Linux machine with one or more cores. The results explained the performance of a single core and parallel processing efficiency of the KISTI-5 supercomputer (the Nurion KNL and the SKL). When using a single core, the CPU time, and wall clock time of the SKL were found to be smaller than those of the KNL and the local Linux machine.

When using one node (multiple cores), the wall clock time of the KNL, the SKL, and the local Linux machine was reduced compared to that when using one core. Because the performance per core of the KNL was inferior to that of the SKL and the local Linux machine, optimization, and parallelization must be considered with a large number of the KNL cores. The results can help optimize the HEP software using high-performance computing (HPC) and enable the users to implement parallel processing.

ORCID

Kihong Park   https://orcid.org/0000-0003-0567-3493
Kihyeon Cho   https://orcid.org/0000-0003-1705-7399

REFERENCES

Aad G, Abajyan T, Abbott B, Abdallah J, Khalek SA, et al., Observation of a new particle in the search for the standard model higgs boson with the ATLAS detector at the LHC, Phys. Lett. B. 716, 1-29 (2012). https://doi.org/10.1016/j.physletb.2012.08.020

Alves D, Arkani-Hamed N, Arora S, Bai Y, Baumgart M, et al., Simplified models for LHC new physics searches, J. Phys. G. Nucl. Part. Phys. 39, 105005 (2012). https://doi.org/10.1088/0954-3899/39/10/105005

Alwall J, Frederix R, Frixione S, Hirschi V, Maltoni F, et al., The automated computation of tree-level and next-to-leading order differential cross sections, and their matching to parton shower simulations, J. High. Energ. Phys. 2014, 79 (2014). https://doi.org/10.1007/JHEP07(2014)079

Antcheva I, Ballintijn M, Bellenot B, Biskup M, Brun R, et al., Root—A C++ framework for petabyte data storage, statistical analysis and visualization, Comp. Phys. Comm. 180, 2499-2512 (2009). https://doi.org/10.1016/j.cpc.2009.08.005

Chatrchyan S, Khachatryan V, Sirunyan AM, Tumasyan A, Adam W, et al., Observation of a new boson at a mass of 125 GeV with the CMS experiment at the LHC, Phys. Lett. B. 716, 30-61 (2012). https://doi.org/10.1016/j.physletb.2012.08.021

Cho K, Computational science and the search for dark matter, New. Phys. Sae. Mulli. 66, 950-956 (2016a). https://doi.org/10.3938/NPSM.66.950

Cho K, e-Science paradigm for astroparticle physics at KISTI, J. Astron. Space. Sci. 33, 63-67 (2016b). https://doi.org/10.5140/JASS.2016.33.1.63

Cho K, Computational science-based research on dark matter at KISTI, J. Astron. Space. Sci. 34, 153-159 (2017). https://doi.org/10.5140/JASS.2017.34.2.153

Choi W, Cho K, Yeo I, Performance profiling for brachytherapy applications, Comp. Phys. Comm. 226, 180-186 (2018). https://doi.org/10.1016/j.cpc.2017.12.022

Conte E, Fuks B, Serret G, Madanalysis 5, a user-friendly framework for collider phenomenology, Comp. Phys. Comm. 184, 222-256 (2013). https://doi.org/10.1016/j.cpc.2012.09.009

De Favereau J, Delaere C, Demin P, Giammanco A, Lemaître V, et al., Delphes 3: a modular framework for fast simulation of a generic collider experiment, J. High Energ. Phys. 2014, 57 (2014). https://doi.org/10.1007/JHEP02(2014)057

Shuve B, Yavin I, Dark matter progenitor: light vector boson decay into sterile neutrinos, Phys. Rev. D, 89, 113004 (2014). https://doi.org/10.1103/PhysRevD.89.113004

Sjöstrand T, Ask S, Christiansen JR, Corke R, Desai N, et al., An introduction to PYTHIA 8.2, Comp. Phys. Comm. 191, 159-177 (2015). https://doi.org/10.1016/j.cpc.2015.01.024

Yeo I, Cho K, Researches on dark matter using $e^+ e^-$ collider, J. Astron. Space Sci. 35, 67-74 (2018). https://doi.org/10.5140/JASS.2018.35.2.67

Yeo I, Cho K, Study on geant4 simulation toolkit using a low energy physics profiling system, J. Korean Phys. Soc. 74, 923-929 (2019). https://doi.org/10.3938/jkps.74.923

Yeo I, Cho K, Low-energy physics profiling of the geant4 simulation tool kit on evolving computing architectures, J. Korean Phys. Soc. 76, 1047-1053 (2020). https://doi.org/10.3938/jkps.76.1047